The Astrophysical Journal, 933:137 (11pp), 2022 July 10 https://doi.org/10.3847/1538-4357/ac75d3

The Common Envelope Evolution Outcome—A Case Study on Hot Subdwarf B Stars

Hongwei Ge[1,2,3], Christopher A. Tout[2], Xuefei Chen[1,3], Matthias U. Kruckow[1,3], Hailiang Chen[1,3], Dengkai Jiang[1,3], Zhenwei Li[1,3], Zhengwei Liu[1,3], and Zhanwen Han[1,3]

[1] Yunnan Observatories, Chinese Academy of Sciences, 396 YangFangWang, Guandu District, Kunming, 650216, People's Republic of China; gehw@ynao.ac.cn, cat@ast.cam.ac.uk, zhanwenhan@ynao.ac.cn

[2] Institute of Astronomy, The Observatories, University of Cambridge, Madingley Road, Cambridge, CB3 0HA, UK; cxf@ynao.ac.cn

[3] Key Laboratory for Structure and Evolution of Celestial Objects, Chinese Academy of Sciences, P.O. Box 110, Kunming 650216, People's Republic of China

Received 2022 May 19; revised 2022 June 2; accepted 2022 June 3; published 2022 July 11

Abstract

Common envelope evolution (CEE) physics plays a fundamental role in the formation of binary systems, such as merging stellar gravitational wave sources, pulsar binaries, and Type Ia supernovae. A precisely constrained CEE has become more important in the age of large surveys and gravitational wave detectors. We use an adiabatic mass-loss model to explore how the total energy of the donor changes as a function of the remnant mass. This provides a more self-consistent way to calculate the binding energy of the donor. For comparison, we also calculate the binding energy through integrating the total energy from the core to the surface. The outcome of CEE is constrained by total energy conservation at the point at which both components' radii shrink back within their Roche lobes. We apply our results to 142 hot subdwarf binaries. For shorter orbital period hot subdwarf B stars (sdBs), the binding energy is highly consistent. For longer orbital period sdBs in our samples, the binding energy can differ by up to a factor of 2. The common envelope (CE) efficiency parameter $\beta_{\rm CE}$ becomes smaller than $\alpha_{\rm CE}$ for the final orbital period $\log_{10} P_{\rm orb}/{\rm days} > -0.5$. We also find the mass ratios $\log_{10} q$ and CE efficiency parameters $\log_{10} \alpha_{\rm CE}$ and $\log_{10} \beta_{\rm CE}$ linearly correlate in sdBs, similarly to the findings of De Marco et al. for post-AGB binaries.

Unified Astronomy Thesaurus concepts: Common envelope evolution (2154); Stellar physics (1621); Stellar evolution (1599); Binary stars (154)

1. Introduction

Binary star evolution plays an essential role in the formation of almost all energetic and exotic objects in astrophysics. This hinges not only on the binary fraction being over half of all stellar systems (Duchêne & Kraus 2013; Moe & Di Stefano 2017) but also the existence of binary interactions, such as Roche-lobe overflow and common envelope evolution (CEE). CEE was initially proposed to explain the formation of short orbital period cataclysmic binaries (Webbink 1975; Paczynski 1976). Subsequently it has been found that CEE plays a fundamental role in the formation of binary systems with at least one compact component, a white dwarf (WD), neutron star, or black hole. These include merging stellar gravitational wave sources (Taam & Sandquist 2000; Nelemans et al. 2001), pulsar binaries (Portegies Zwart & Yungelson 1998), and Type Ia supernovae (Webbink 1984).

A common envelope (CE) phase is believed to form when a giant donor star, with a deep convective envelope, transfers its mass to a less-massive companion star (Paczynski 1976). The outcome of a CE phase can be either the formation of a short orbital period compact binary in the case of a successful envelope ejection or the formation of a merged star in the case of a failure of envelope ejection (see Figure 1).

Generally speaking, there are two different approaches aimed at improving the CEE physics. The first is 3D hydrodynamic simulations. Significant progress has been made recently by addressing proper numerical methods and more precise physics. For examples, Ricker & Taam (2012) used both a piecewise parabolic method and an adaptive mesh refinement method in CE studies; Ricker et al. (2019) considered radiation transport effects in CE simulations; Sand et al. (2020; and references therein) examined the ionization energy contribution to the CE ejection process; Lau et al. (2022) performed adiabatic simulations including both radiation energy and recombination energy. Gonzalez-Bolivar et al. (2022) simulated the CE process between a thermally pulsating asymptotic giant branch star and a low-mass main-sequence (MS) star and found that (1) the inclusion of recombination energy results in wider separations and (2) thermal pulses can trigger CEs and lead to the prediction of a larger population of post-CE binaries. But a successful ejection of the whole envelope is still facing challenges. The second approach is a stellar evolution method. The standard procedure to predict the outcome of CEE is known as the energy formalism (Webbink 1984; Iben et al. 1984; Livio & Soker 1988). This is based on the essential physics of total energy *conservation*. The initial and final total energy of the binary system $E_{\rm i}$ and $E_{\rm f}$ are assumed to be conserved.

$$E_{\rm i} = E_{\rm f} \tag{1}$$

with

$$E_{\rm i} = E^{\rm i}_{\rm orb} + E_{\rm 1i} + E_{\rm 2i}, \tag{2}$$

and

$$E_{\rm f} = E^{\rm f}_{\rm orb} + E_{\rm 1f} + E_{\rm 2f}. \tag{3}$$

The right parts of Equations (2) and (3) are the orbital energy of the binary system and the total self energy of the donor and accretor. Typically for an MS or WD accretor E_2 is assumed not to change. In this standard prescription a CE efficiency

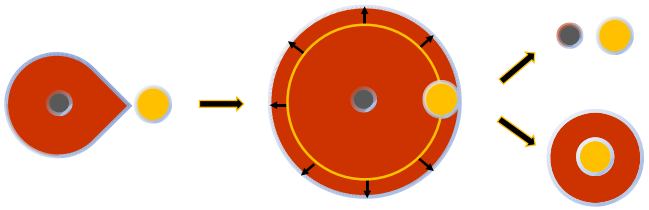

Figure 1. Common envelope evolution (CEE), not to scale. A giant unstably overflows on to a more compact companion. If the envelope can be ejected a close binary results. Otherwise the stars merge.

parameter $\alpha_{\rm CE}$ is introduced as the fraction of the orbital energy change $\Delta E_{\rm orb}$ that is used to overcome the binding energy $E_{\rm bind,}$ so that

$$\alpha_{\rm CE}\Delta E_{\rm orb} = \Delta E_1 = E_{\rm bind}. \quad (4)$$

This formula is popularly written as (Webbink 1984, 2008; de Kool 1990)

$$\alpha_{\rm CE}\left(-\frac{GM_{1\rm i}M_2}{2a_{\rm i}} + \frac{GM_{1\rm f}M_2}{2a_{\rm f}}\right) = \frac{GM_{1\rm i}M_{1\rm e}}{\lambda R_{1\rm i}}, \quad (5)$$

where G is Newton's gravitational constant, M are the masses, a are the semimajor axes, R is the stellar radius, and λ is a dimensionless parameter that reflects the structure of the star. The 1 and 2 subscripts refer to the donor and accreter, respectively. The subscripts i and f refer to the initial and final state of the CE phase. $M_{1\rm e} = M_{1\rm i} - M_{1\rm f}$ is the mass of the CE.

The constraints on the onset, the outcome of CEE physics, and other basic knowledge of binary interactions can be used as physical inputs for binary population synthesis (BPS) studies. Hjellming & Webbink (1987) used polytropic stellar models to predict the critical initial mass ratios for dynamical timescale mass transfer, and Soberman et al. (1997) further extended this to nonconservative cases. Chen & Han (2003, 2008) used Cambridge STARS code and Pavlovskii & Ivanova (2015) and Pavlovskii et al. (2017) used the MESA code to provide limits on the onset of the CE process. Ge et al. (2010a, 2010b, 2015, 2020a, 2020b) built the adiabatic and thermal equilibrium mass-loss models and provided the critical initial mass ratios for dynamical timescale or thermal timescale mass transfer. Besides the BPS studies on low-mass binary stars (e.g., Lagos et al. 2020; Hernandez et al. 2021; Leiner & Geller 2021), such studies for massive binary stars have increased recently. For examples, studies cover pulsating ultraluminous X-ray sources (Misra et al. 2020), close double neutron star sources (Vigna-Gómez et al. 2020; Kruckow 2020; Mandel et al. 2021), neutron star binaries through accretion-induced collapse (Wang & Liu 2020), compact intermediate-mass black hole X-ray binaries (Chen 2020), luminous red novae (Blagorodnova et al. 2021), rapidly rotating Be binaries (El-Badry & Quataert 2021), short-period massive binary stars (Sen et al. 2022), Type II supernova progenitors (Zapartas et al. 2021), and black hole or neutron star binaries (recent papers like Shao & Li 2021; Mandel & Broekgaarden 2022). Marchant et al. (2021) focuses on 30 $M_\odot$ models, while Kruckow et al. (2016) focuses on 80–88 $M_\odot$ models. Most of recent studies are driven by the detection of gravitational wave mergers (Abbott et al. 2016, 2017, 2021). These observed binary objects need precisely constrained CEE physics.

However, the detailed physics of the CEE outcome (see the recent review by Ivanova et al. 2020) is still far from well understood. Many authors provide useful constraints on an efficiency parameter $\alpha_{\rm CE}$ (e.g., Zorotovic et al. 2010; De Marco et al. 2011), a structure parameter λ, or the binding energy (e.g., Dewi & Tauris 2000; Xu & Li 2010). These studies are based on detailed calculations and provide the physical parameters as functions of stellar mass and evolutionary state. We provide here an alternative way to calculate the new binding energy from the difference between the initial and final total energy of the donor star (Ge et al. 2010a). We investigate how the companion mass impacts the binding energy for a donor with the same mass and evolutionary state. We try to answer the question of whether there is a universal constant CE efficiency (Ivanova et al. 2020) $\alpha_{\rm CE}$ through observed short-period hot subdwarf B stars (sdBs).

In Section 2, we describe our method. In Section 3, we introduce short orbital period sdBs from both theoretical and observational viewpoints. We present results and discussions of the CE efficiency parameters with binding energy derived from our standard formula and our new algorithm in Section 4. We summarize and conclude on constraints on CEE outcomes in Section 5.

2. Numerical Methods

We use our code based on our adiabatic mass-loss model (Ge et al. 2010a, 2010b, 2015, 2020a) to investigate how the total energy varies as a function of the donor's remaining mass. The code replaces the luminosity and temperature equations with a frozen entropy profile to give the approximate response of a donor star undergoing very rapid mass transfer. The basic philosophy of the adiabatic mass-loss code is the same as the Cambridge STARS code (Eggleton 1971, 1972, 1973) and a simplified version of it (Paxton 2004). The input physics, such as the equation of state, opacity, and nuclear reaction rates, is the same as in the STARS code (Pols et al. 1998). We set the mixing-length parameter to be $\alpha = l/H_P = 2.0$, the ratio of mixing length l to pressure scale height H_P, and the convective overshooting parameter $\delta_{\rm ov} = 0.12$ (Pols et al. 1998).

We build a grid of initial stellar models with masses 1.0, 1.3, 1.6, 1.8, and 2.0 $M_\odot$ and metallicity $Z = 0.02$ (see Figure 2). The change of the total energy of the donor is calculated by (see Ge et al. 2010a)

$$E_{\rm bind} = \int_0^{M_{1\rm f}}\left(-\frac{Gm}{r} + U\right)dm - \int_0^{M_{1\rm i}}\left(-\frac{Gm}{r} + U\right)dm, \quad (6)$$

where m is the mass, r is the radius, and U is its specific internal energy. Combining Equations (4)–(6), we find the initial to final separation relation,

$$\frac{a_{\rm f}}{a_{\rm i}} = \frac{M_{1\rm f}}{M_{1\rm i}}\left(1 + \frac{2a_{\rm i}\Delta E_1}{\beta_{\rm CE}GM_2M_{1\rm i}}\right)^{-1}. \quad (7)$$

Here, we define the CE efficiency parameter as $\beta_{\rm CE}$ to indicate that the binding energy is calculated by Equation (6), which considers the response and the redistribution of the core and the thin envelope. This can differ somewhat from that of the initial stellar model, particularly for more-massive stars with a nondegenerate core (Ge et al. 2010a; Deloye & Taam 2010).

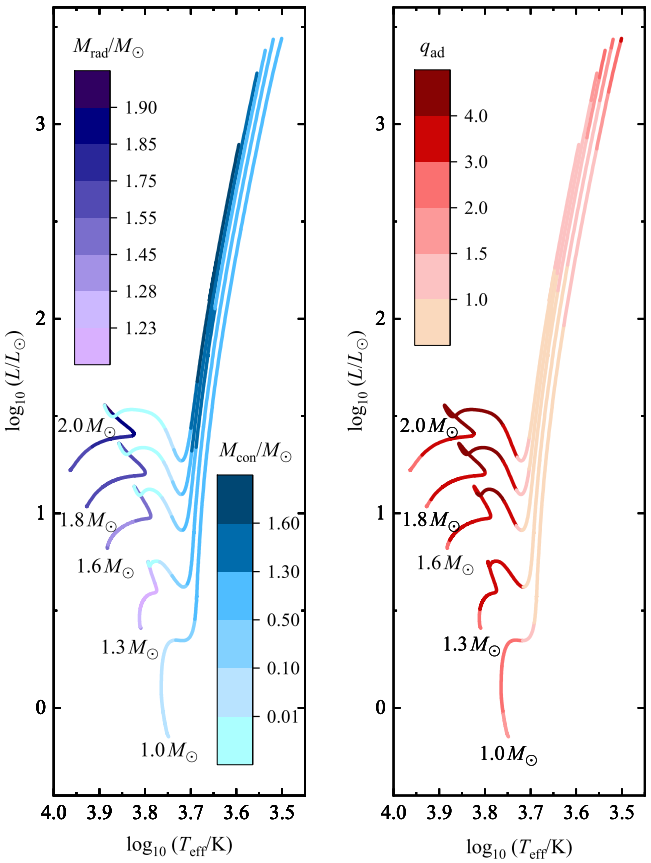

Figure 2. The Hertzsprung–Russell diagram of low-mass donor stars. The colors in the left panel indicate the mass of the convective or radiative envelope. The colors in the right panel show the critical initial mass ratio for dynamical timescale mass transfer (Ge et al. 2015, 2020a). The tracks are for stars of 1.0, 1.3, 1.6, 1.8, and 2.0 $M_\odot$ from bottom to top. To avoid confusion, data ends at the tip of the red giant branch (TRGB).

For comparison, we also calculate the binding energy from

$$E'_{\rm bind} = -\int_{M_{\rm He}}^{M_{\rm 1i}} \left(-\frac{Gm}{r} + U\right) dm, \tag{8}$$

and $M_{\rm He}$ is the helium core mass where the mass fraction of hydrogen is 0.1. We also transfer this binding energy to the corresponding structure parameter λ (see Table 1) through $E'_{\rm bind} = GM_{\rm 1i}M_{\rm 1e}/\lambda R_{\rm 1i}$. In this case, the corresponding CE efficiency parameter $\alpha_{\rm CE}$ is the same as in Equation (5).

The initial separation $a_{\rm i}$ can be found, from the donor star's mass $M_{\rm 1i}$ and radius $R_{\rm 1i} = R_{\rm L}$ (requiring the donor to fill its Roche lobe at the onset of the CE) with companion mass M_2, to be

$$a_{\rm i} = \frac{R_{\rm 1i}}{r_{\rm L}(M_{\rm 1i}/M_2)}, \tag{9}$$

where $R_{\rm 1i}$ is the radius of the giant donor when it first fills its Roche lobe. For sdBs we take this to be the radius at the tip of the red giant branch (TRGB),[4] and, by Eggleton's approximation for Roche-lobe radius (Eggleton 1983),

$$r_{\rm L}(q) = \frac{0.49q^{2/3}}{0.6q^{2/3} + \ln(1+q^{1/3})} = \frac{R_{\rm L}}{a}. \tag{10}$$

The final separation $a_{\rm f}$ can be determined from an observed object's orbital period if we assume the period and semimajor axis did not change between the end of the CE and the observation:

$$P^2_{\rm orb} = \frac{4\pi^2 a_{\rm f}^3}{G(M_{\rm 1f} + M_2)}. \tag{11}$$

The outcome of CEE can be self-consistently constrained by total energy conservation (Equation (7)) at the point at which both components' radii shrink back within their Roche lobes, $R_{\rm 1f} \leqslant R_{\rm 1,L_1}$ and $R_2 \leqslant R_{\rm 2,L_1}$ (see also Ge et al. 2010a).

Table 1
Parameters about Three TRGB Stars

$M_{\rm 1i}$ $M_\odot$	$M_{\rm He}$ $M_\odot$	$\log_{10}R_{\rm 1i}$ $R_\odot$	Z	$E'_{\rm bind}$ erg	λ
1.0	0.4620	2.2425	0.02	2.548×10^{46}	0.4580
1.3	0.4615	2.2035	0.02	3.029×10^{46}	0.8540
1.6	0.4559	2.1394	0.02	4.235×10^{46}	1.1895

3. Short Orbital Period sdBs

Subdwarf B stars (sdBs) are core helium-burning stars with masses around 0.5 $M_\odot$ and a thin hydrogen-rich envelope (less than 0.02 $M_\odot$). They are hot and their effective temperature is between 20,000 and 40,000 K (Heber 2009). So sdBs emit strong ultraviolet (UV) emission and this makes them the major source of the UV-upturn in the elliptical galaxies (Ferguson et al. 1991; Han et al. 2007). About half of sdBs are in close binaries with a WD or low-mass MS companion star (Heber 2009). The most-favored formation channels for sdBs are the CE ejection channel, the stable Roche-lobe overflow channel, and the merging double helium WD channel (Han et al. 2002, 2003). The merging channel produces isolated sdBs and the first two provide sdBs in binaries. The CEE with a substellar companion can also form an isolated sdB (Soker 1998; Kramer et al. 2020). Besides their importance in binary evolution, sdBs are also useful for asteroseismology (e.g., Fontaine et al. 2003), cosmology (Justham et al. 2009; Wang 2018), and gravitational wave sources studies (Wu et al. 2018).

Recently, many sdBs have been found in survey projects, such as Gaia (Geier et al. 2019) and LAMOST (Luo et al. 2021). However, a strict constraint on the orbital parameters and masses of both components is still lacking. So we use sdB examples provided by Kupfer et al. (2015) to carry out our study. Through detailed stellar evolution studies, Han et al. (2002) and Zhang et al. (2021) find that the low-mass progenitor models of short orbital period sdBs are located almost at the TRGB in order to trigger a helium flash. Furthermore, the CE ejection scenario is the only likely formation channel for these short-period sdB binaries below 10 days (Maxted et al. 2001). Hence, the simplicity of these sdBs' progenitors makes them the perfect objects to constrain CEE physics.

Kupfer et al. (2015) studied 142 short-period sdB binaries, including 12 new systems. Assuming a canonical mass for the

[4] If a progenitor overfills its Roche lobe near the TRGB and suffers a CE ejection, the remnant core can trigger a delayed helium flash and finally form an sdB (Han et al. 2002). So, we set $R_{\rm 1i} = R_{\rm TRGB}$.

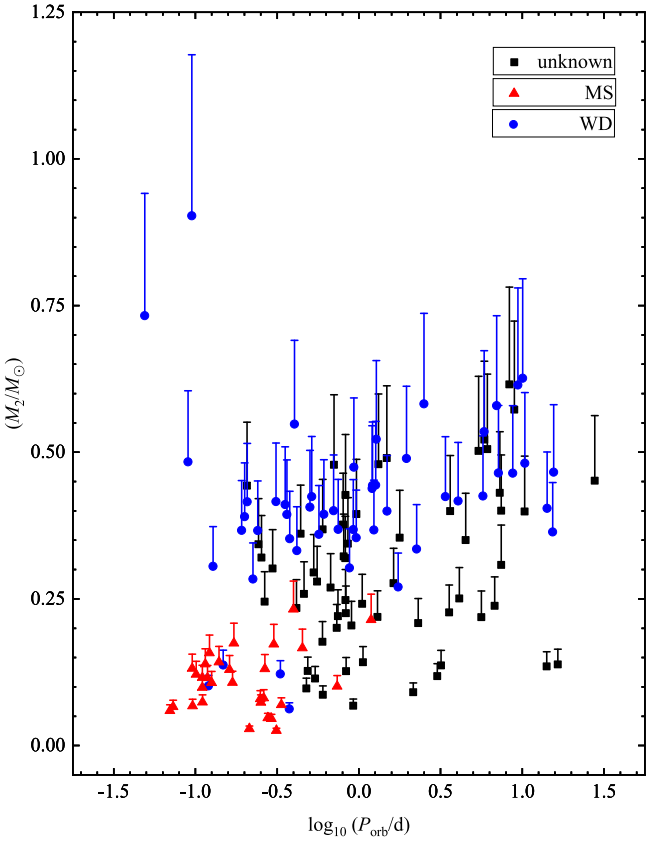

Figure 3. The orbital periods against the companion masses of 142 observed hot subdwarf B stars (sdBs). As described by Kupfer et al. (2015), different symbols indicate the minimum companion masses, assuming the sdB mass $M_{\rm sdB} = 0.47\,M_\odot$ and the inclination angle $i = 90°$. A mean companion mass, the upper error bar, can be found assuming an inclination angle $i = 60°$. Black squares, red triangles, and blue circles show the type of the companion star, unknown, main-sequence (MS), or white dwarf (WD), respectively.

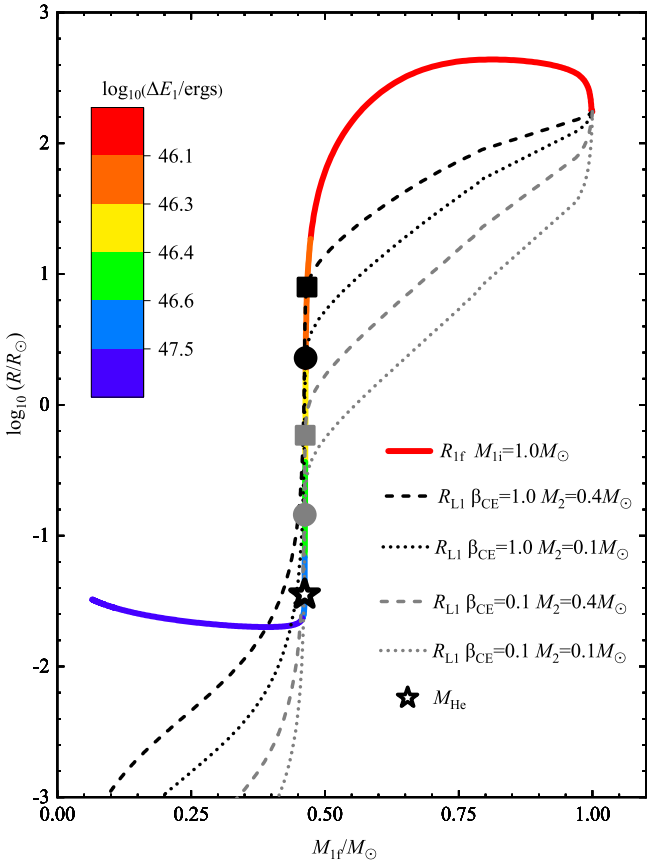

Figure 4. The remnant radius (colored line) and Roche-lobe radius (dashed and dotted lines) as a function of mass. The initial model is a 1.0 $M_\odot$ star at the TRGB. Dashed and dotted lines (solving Equations (7) to (11) of this paper and Equation (1) of Kupfer et al. (2015) correspond to companion masses of 0.4 and 0.1 $M_\odot$. Black and gray colors indicate efficiency parameters $\beta_{\rm CE}$ of 1.0 and 0.1. Filled squares and filled circles locate the outcome of the CEE with the given efficiency parameter $\beta_{\rm CE}$ and companion mass M_2. The pentagram is the helium core mass $M_{\rm He}$ where the mass fraction of hydrogen is 0.1.

sdB $M_{\rm sdB} = 0.47\,M_\odot$ (Fontaine et al. 2012) and inclination angles of $i = 90°$ and 60°, the minimum and mean mass of the companion can be determined by solving the equation for the mass function (Figure 3). Kupfer et al. (2015) find that a peak around $0.1\,M_\odot$ corresponds to the low-mass MS companions and another peak around $0.4\,M_\odot$ corresponds to the WD companions (see their Figure 8). Again, these short-period sdB binaries are most likely formed from CEE and we use them to constrain its physics in the next section.

4. Results and Discussions

We present CE efficiency parameters as a function of the orbital period for 142 sdB binaries. Three different TRGB donor stars are explored. Their binding energies are calculated by either integrating from the core to the surface of the initial model when CEE begins $E'_{\rm bind}$ (Equation (8)) or the change of total energy during CEE $E_{\rm bind}$ (Equation (6)). The corresponding CE efficiency parameters are written as $\alpha_{\rm CE}$ and $\beta_{\rm CE}$, respectively. For shorter orbital period sdBs, the binding energy is almost the same and we find the difference between $\alpha_{\rm CE}$ and $\beta_{\rm CE}$ is small. For longer orbital period sdBs in our samples we have found that the binding energy can differ by up to a factor of 2. The CE efficiency parameter $\beta_{\rm CE}$ becomes smaller than $\alpha_{\rm CE}$ for final orbital periods $\log_{10} P_{\rm orb}/{\rm d} > -0.5$. A shallower slope for $\log_{10}\beta_{\rm CE}$ with $\log_{10} P_{\rm orb}$ than that for $\log_{10}\alpha_{\rm CE}$ is found for sdBs with all types of companion.

4.1. 1.0 $M_\odot$ TRGB Donor Star

According to the initial mass function (e.g., Zorotovic et al. 2010) lower-mass stars dominate the progenitors of sdBs. So we take a 1.0 $M_\odot$ TRGB donor star as the typical progenitor of an sdB. The initial mass and radius of the donor are known. The final orbital period after CE ejection is found from the observed sdB binary. How the total energy changes as a function of remnant mass can be calculated through our adiabatic mass-loss code. With an initial guess and bisection method to solve the Equations (7) to (11) of this paper and Equation (1) of Kupfer et al. (2015) we can find the CE parameter $\beta_{\rm CE}$ that satisfies the sdB mass $M_{\rm sdB}$, minimum companion mass M_2 (assuming $i = 90°$) and the orbital period $P_{\rm orb}$. For comparison, we also calculate $E'_{\rm bind}$ in place of Equation (6) and solve for the CE parameter $\alpha_{\rm CE}$.

The solid line in Figure 4 demonstrates how the radius responds to mass loss when we assume the CE envelope is ejected adiabatically. The color of the solid line shows the binding energy as a function of the star's remnant radius R_{1f} and mass M_{1f}. The dashed and dotted lines show how the inner Roche-lobe radius R_L changes for companion masses of 0.4 and $0.1\,M_\odot$. The black and gray colors refer to the CE efficiency parameters of 1.0 and 0.1. As discussed in Section 2, the symbols are located where the remnant stars just shrink

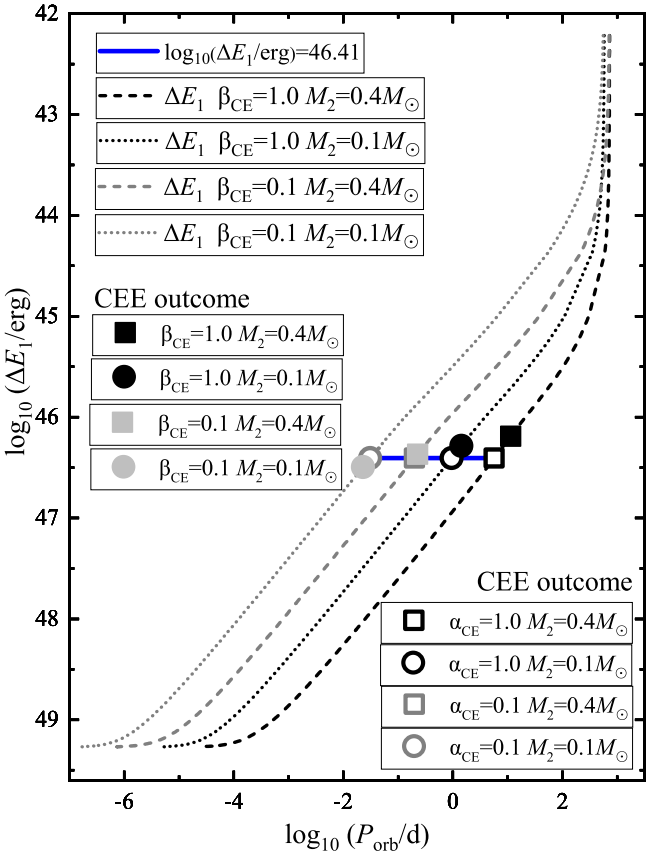

Figure 5. The binding energy as a function of orbital period. The initial model is a 1.0 $M_\odot$ star at the TRGB. Dashed and dotted lines (solving Equations (7) to (11) of this paper and Equation (1) of Kupfer et al. (2015)) correspond to companion masses of 0.4 and 0.1 $M_\odot$. Black and gray colors indicate efficiency parameters $\beta_{\rm CE}$ of 1.0 and 0.1. Filled ($\beta_{\rm CE}$) and open ($\alpha_{\rm CE}$) symbols locate the outcome of the CEE with the given efficiency parameter and companion mass. Filled symbols correspond to each other between Figures 4 and 5. The blue line is the binding energy from the right-hand side of Equation (5) for $\lambda = 0.458$.

back inside their Roche lobes. Lines and symbols in Figure 5 have the same meaning. For a specified progenitor with a given mass and evolutionary stage, the binding energy is not constant (the blue line in Figure 5 is for $\lambda = 0.458$) as people often assumed. The binding energy varies with both the efficiency parameter $\beta_{\rm CE}$ and the companion mass M_2 (Figure 5), as well as the rebalancing of the remnant star after its envelope mass is ejected. The difference between binding energies $E_{\rm bind}$ and $E'_{\rm bind}$ becomes larger for longer orbital period sdBs, and higher companion masses if the CE efficiency parameters $\alpha_{\rm CE}$ and $\beta_{\rm CE}$ are the same. Consequently, although the final mass is nearly the same as the helium core mass $M_{\rm He}$, defined by where the mass fraction of hydrogen is 0.1 (pentagram in Figure 4), the final radii differ from each other by orders of magnitude (see symbols in Figure 4). The remnant core masses are all slightly larger than the helium core mass. Although the hydrogen envelope is very thin, the surface hydrogen and helium mass fractions are still similar to its progenitor's surface.

Figures 6 to 9 present the CE efficiency parameters $\alpha_{\rm CE}$ (open symbols) and $\beta_{\rm CE}$ (filled symbols) as functions of the orbital period of observed sdBs, of which the companions are MS, WD, or unknown (MS/WD) stars. The progenitor donor is a 1.0 $M_\odot$ TRGB star and the companion mass M_2 is solved with an inclination angle of $i = 90°$. The dashed and solid lines are linear least-squares fits to the data (see Table 2). Figures 6–9 indicate that the CE efficiency parameters $\log_{10}\alpha_{\rm CE}$ and

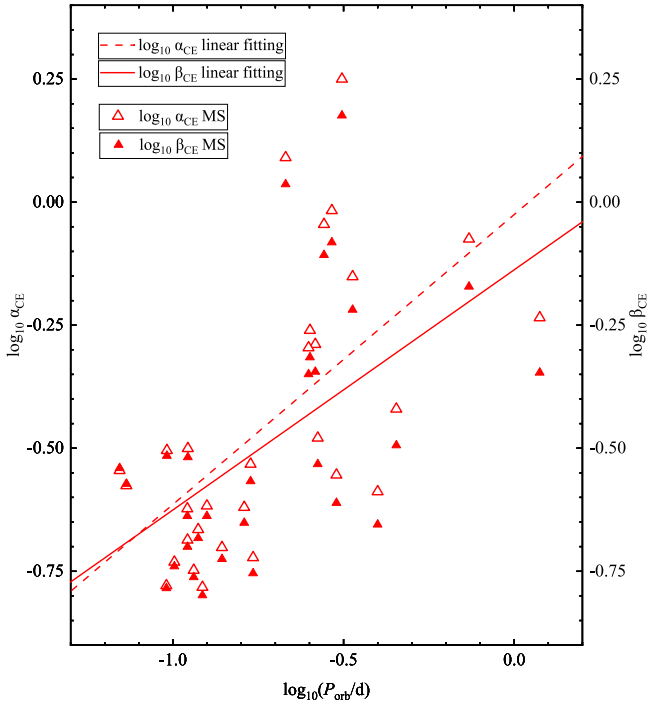

Figure 6. The CE efficiency parameters $\alpha_{\rm CE}$ (open symbols) and $\beta_{\rm CE}$ (filled symbols) against the orbital period of observed sdBs with an MS companion. The initial model is a 1.0 $M_\odot$ TRGB star (other initial models are considered in Figures 10 to 12). The companion mass M_2 is solved with an inclination angle of $i = 90°$. The dashed and solid lines are a linear least-square fits to the data.

$\log_{10}\beta_{\rm CE}$ change linearly with the logarithm of the final orbital period if we assume the progenitor was the same. For short orbital period sdBs the CE efficiency parameters $\log_{10}\alpha_{\rm CE}$ and $\log_{10}\beta_{\rm CE}$ are similar. However, a shallower slope is found for $\log_{10}\beta_{\rm CE}$ than for $\log_{10}\alpha_{\rm CE}$ in all cases for long orbital period sdBs. This agrees with our expectation from Figure 5 because the same progenitor $E_{\rm bind}$ gets much smaller than $E'_{\rm bind}$ for longer orbital period sdBs. Hence, $\beta_{\rm CE}$ becomes less than $\alpha_{\rm CE}$ at longer orbital periods of sdBs. The binding energy $E_{\rm bind}$ from our calculation also becomes important for these long orbital period sdBs.

4.2. 1.0, 1.3, and 1.6 $M_\odot$ TRGB Donor Star

We extend our studies on the CE efficiency parameters for TRGB stars to different mass, $1.3M_\odot$ and $1.6M_\odot$, progenitors. Figures 10 to 12 present both the CE parameters $\alpha_{\rm CE}$ (solid lines) and $\beta_{\rm CE}$ (dashed line) as functions of the orbital periods of observed sdBs with MS, WD, and unknown companions. For each line, the progenitor's initial mass changes from 1.0 $M_\odot$ (bottom) to 1.6 $M_\odot$ (top). Figure 13 presents the weighted CE parameter $\alpha_{\rm CE}$ (open symbols) and $\beta_{\rm CE}$ (filled symbols). The weight factor is $N(M_{\rm 1i}, a_{\rm i}) = M_{\rm 1i}^{-2.7}/a_{\rm i}$ according to the initial mass function, flat distribution of initial mass ratio, and flat distribution of logarithmic initial separation (see Hall & Tout 2014). We find the difference between $\alpha_{\rm CE}$ and $\beta_{\rm CE}$ becomes important for sdBs with orbital periods $P_{\rm orb}$ such that $\log_{10}(P_{\rm orb}/{\rm d}) > -0.5$. For different progenitor masses of short orbital period sdB binaries, the binding energies $E_{\rm bind}$ and $E'_{\rm bind}$ differ significantly for $\log_{10}(P_{\rm orb}/{\rm d}) > -0.5$ with any type of companion. A higher companion mass spirals in and ejects the envelope with a larger final radius and mass, so a smaller binding energy $E_{\rm bind}$ leads to a smaller $\beta_{\rm CE}$.

Table 2
Fitting Parameters of Different Types of Companions

Type	Efficiency	Intercept Value	Standard Error	Slope Value	Standard Error	Adj. R-square
MS	$\log_{10}\alpha_{\rm CE}$	−0.02515	0.11047	0.58893	0.14319	0.35437
MS	$\log_{10}\beta_{\rm CE}$	−0.15583	0.10001	0.47214	0.12962	0.29725
WD	$\log_{10}\alpha_{\rm CE}$	−0.49692	0.02341	0.61430	0.03590	0.85120
WD	$\log_{10}\beta_{\rm CE}$	−0.60204	0.02289	0.50816	0.03511	0.80345
unknown	$\log_{10}\alpha_{\rm CE}$	−0.34292	0.02740	0.62956	0.04982	0.72893
unknown	$\log_{10}\beta_{\rm CE}$	−0.45605	0.02532	0.51224	0.04603	0.67553

Notes. 1. Standard error was scaled with square root of reduced Chi-square.
2. R-square equals $1-\sum_{i=1}^{n}(y_i-f_i)^2/\sum_{i=1}^{n}(y_i-\bar{y})^2$ where n is the total number of these 142 sdBs, y_i is the logarithmic of CE efficiency, f_i is the fitted value, and $\bar{y}$ is the mean of y_i.

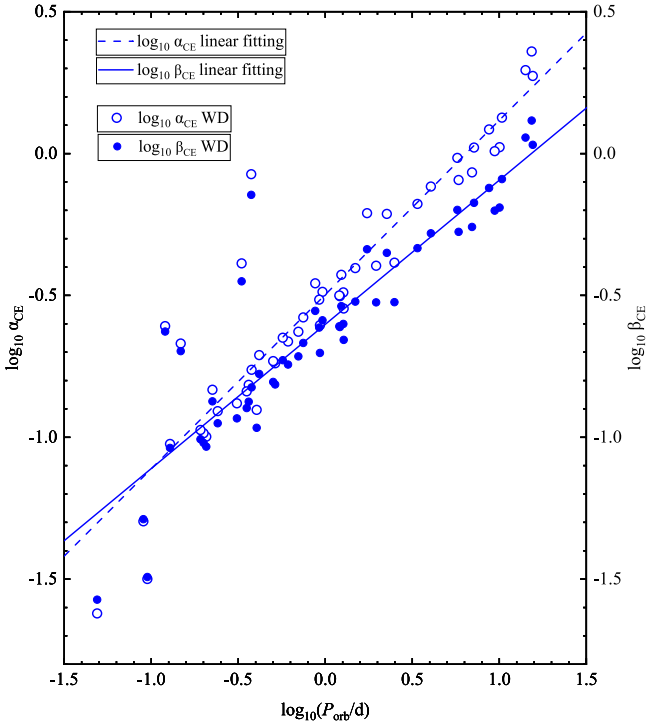

Figure 7. Similar to Figure 6 but for sdBs with a WD companion.

4.3. Influence of the Binding Energy

We assume the outcome of CEE is determined by energy conservation and when both components shrink within their Roche lobes. These last two subsections provide a better understanding of the effects of different binding energy calculation methods. For accuracy, in the standard prescription of the energy formula, we calculate the binding energy $E'_{\rm bind}$ from Equation (8) (see gray open triangles in Figure 14). The companion mass and the final orbital period affect the binding energy and subsequently the gradient of the CE efficiency parameter (Figures 6–9; gradient not shown in Figures 10–13). A flatter slope (solid lines) is seen for the new binding energy algorithm than that from a constant $E'_{\rm bind}$ in Figures 6 to 9 and is independent of the companion type.

For a better understanding of the difference between $\alpha_{\rm CE}$ and $\beta_{\rm CE}$, we show the binding energy $E_{\rm bind}$ and $E'_{\rm bind}$ as a function the orbital period for the 142 sdBs in Figure 14. The binding energy $E_{\rm bind}$ is calculated consistently as the envelope is ejected. For a given initial binary system, a shorter final orbital period requires the companion to spiral in more to eject the CE. In such cases the binding energy $E_{\rm bind}$ is close to $E'_{\rm bind}$ because the the final mass is close to the Helium core mass. The binding energy $E_{\rm bind}$ is smaller for a longer orbital period sdBs (blue filled squares in Figure 14) because the companions do not need to spiral in that much. $E_{\rm bind}$ can decrease from $E'_{\rm bind}=2.548\times10^{46}$ to 1.358×10^{46} erg for a 1.0 $M_\odot$ TRGB progenitor.

As shown in Equation (7), a different binding energy corresponds to a different CE efficiency. For an observed sdB system with a given progenitor model, the relation between binding energy and CE parameter is positively linearly correlated. A smaller binding energy $E_{\rm bind}$ reduces the CE efficiency parameter $\beta_{\rm CE}$ more than $\alpha_{\rm CE}$ for $E'_{\rm bind}$ in long orbital period sdBs (Figures 6 to 14).

4.4. Relation between CE Parameter and Mass Ratio

If we reformulate Equation (5), we have the mass ratio ($q=M_{\rm 1i}/M_2$) and CE efficiency relation,

$$\alpha_{\rm CE}=\frac{2q(M_{\rm 1i}-M_{\rm 1f})}{\lambda r_{\rm L}(q)(M_{\rm 1f}a_{\rm i}/a_{\rm f}-M_{\rm 1i})}. \quad (12)$$

Figure 15 shows the initial mass ratios $\log_{10}q$ to CE efficiency $\log_{10}\beta_{\rm CE}$ and $\log_{10}\alpha_{\rm CE}$ relations for short orbital period sdBs. The relation in the top panel is derived from $E'_{\rm bind}$, while that in the bottom panel is derived from $E_{\rm bind}$. We find that there is linear correlation between $\log_{10}q$ and $\log_{10}\alpha_{\rm CE}$ for a given sdB system with different donor masses. Although the relation is stretched for different sdB systems, the linear correlation is universal, sharing the same gradient. We have $\log_{10}\alpha_{\rm CE}=-0.503(\pm0.049)+0.328(\pm0.062)\times\log_{10}q$ with the adjusted R-squared of 0.059 and $\log_{10}\beta_{\rm CE}=-0.631(\pm0.044)+0.400(\pm0.055)\times\log_{10}q$ with the adjusted R-squared of 0.108.

De Marco et al. (2011) explored such an anticorrelation between $\log 1/q$ and $\log\alpha_{\rm CE}$ for postasymptotic giant branch (post-AGB) binaries. They found the gradient to be around −1.2, but they excluded post-RGB donors. The results for sdBs in this paper also show the $\log 1/q$ versus $\log\alpha_{\rm CE}$ anticorrelation (see Equation (12)).

4.5. Effects from Other Sources

To constrain CE efficiency parameters, we use a new binding energy algorithm addressing the influence of the companion mass and the rebalance of the remnant core. The progenitors of short orbital period sdBs are located at a narrow range near the

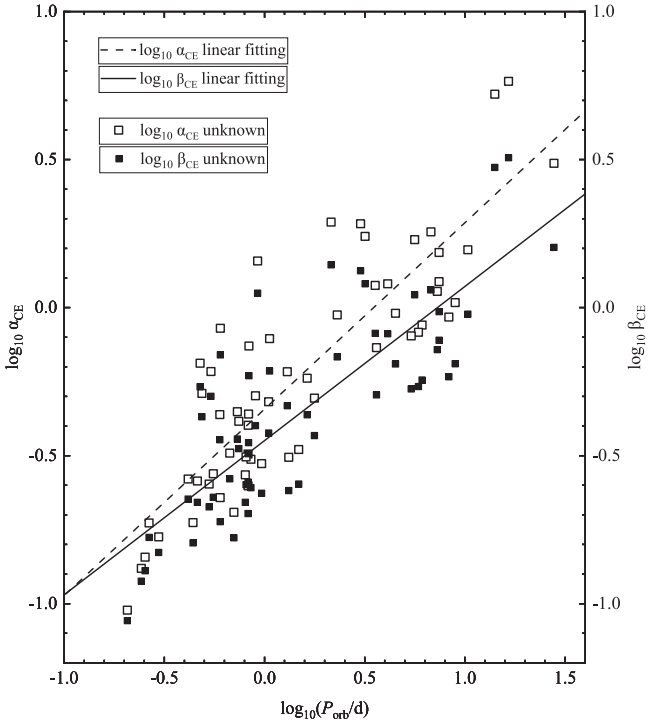

Figure 8. Similar to Figure 6 but for sdBs with an unknown companion.

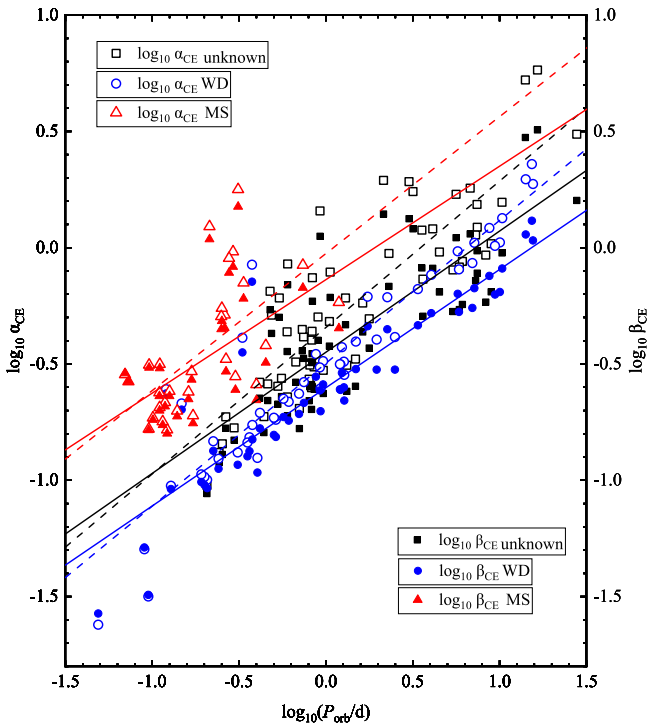

Figure 9. All data in Figures 6–8 combined. The larger CE efficiency parameter for sdBs with MS companions than that for WD companions is because of the smaller companion mass (see Figure 3).

TRGB. We only show the results of TRGB stars in the previous subsections. Progenitors from a slightly earlier stage of TRGB extend a little the range of CE efficiency parameters. The role that convection might play in transporting energy out, as Wilson & Nordhaus (2022) suggest, might affect CEE efficiencies. We discuss other possible effects on the uncertainty of CE efficiency parameters such as metallicity, companion type, and inclination angle in this subsection.

We only explored stars with metallicity $Z = 0.02$. Metal-poor stars are more compact than metal-rich stars with the same mass. We find that metal-poor stars have smaller radii and shorter orbital periods for the same companion mass (Figure 16). The binding energy is highly related to the radius of the donor star. We expect that a metal-poor star has a larger binding energy $E'_{\rm bind}$ than a metal-rich star. For a given CE efficiency parameter $\beta_{\rm CE} = 0.3$, the final orbital period or separation is surprisingly larger for a metal-poor star (see Equation (7)). This is because the compact metal-poor star shrinks to its Roche lobe earlier and makes $E_{\rm bind}$ smaller. So a smaller metallicity tends to reduce the linear slope of the logarithm of the CE efficiency parameter and final orbital period. Unfortunately it is hard to spectrally determine the metallicity of short orbital period hot subdwarf binaries (private communication with Prof. Yangping Luo). For example, the companions of sdBs are all cool stars with a spectral type around *M* (Kupfer et al. 2015) while the sdB is too luminous, unlike the long orbital period sdBs, which indicate the chemical evolution history of the Milky Way (Vos et al. 2020). We currently cannot pick out the observed sdBs with metallicity $Z = 0.02$ to give a stricter prediction or constraint.

The companion mass range is different for short orbital period sdBs with an MS or WD companion (Figure 3). From theoretical analysis, if the MS companion mass M_2 is too close to that of its companion $M_{1\rm i}$ it is likely to merge with the envelope, because the companion's radius is likely to be larger than its Roche-lobe radius (Figure 17), for example, if M_2 were larger than 1.1 $M_\odot$ for a $M_{1\rm i} = 1.6\ M_\odot$ TRGB star with $\beta_{\rm CE} = 0.1$. Furthermore, the MS companion mass cannot be too massive because at the initial mass ratio $q < q_{\rm ad}$, it avoids CEE (right panel of Figure 2). A combination of the above reasons is very likely to explain the lower-mass peak around $0.1\,M_\odot$ in Kupfer et al.'s (2015) Figure 8. There is also a lower limit around 0.1 for the CE efficiency parameters of sdBs with an MS companion. A low-mass MS companion does not shrink inside its Roche-lobe if the CE efficiency parameter is too small (Figure 17). For extreme short orbital period sdBs with a WD companion, the CE efficiency parameters are smaller than 0.1 (Figures 7, 9, 11, and 13). The progenitors of these sdBs are possibly more massive than $2.5\,M_\odot$. They likely form through the CE + CE channel. We only explore the progenitors of sdBs with a degenerate core and our current results do not cover progenitors of sdBs with a nondegenerate core.

In this study, we assume the inclination angle $i = 90°$. We might expect there is a random distribution of the inclination angle, flat in $\cos i$. However, the companion mass is degenerate with the inclination angle (Equation (1) of Kupfer et al. 2015). We might hope to constrain the CE efficiency parameters through checking the random number density of sdBs with respect to inclination angle (see a similar method for millisecond pulsars with a helium WD by Smedley et al. 2014) but the typical companion mass of sdBs is more extended than the neutron star mass in their study. We hope future observations can provide inclination angles and metallicities in short orbital period binaries with a compact companion.

We might not provide a concluding answer for whether there is a universal constant CE efficiency (Ivanova et al. 2020) $\alpha_{\rm CE}$ but we are trying to provide comprehensive studies and discussions on this aspect. Our results tend to support that longer orbital period sdBs are from lower-mass progenitors while shorter orbital period sdBs are from higher-mass

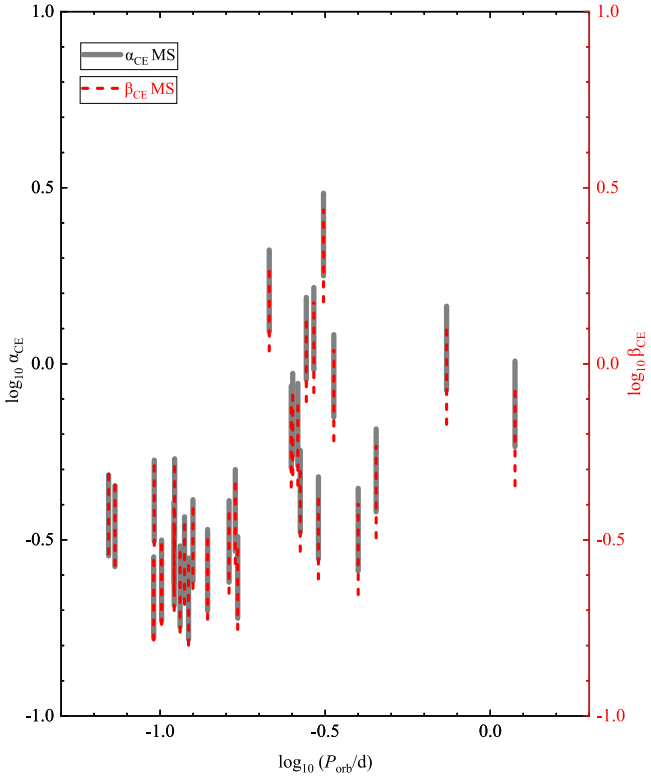

Figure 10. The CE efficiency parameters $\alpha_{\rm CE}$ (gray solid line) and $\beta_{\rm CE}$ (red dashed line) as functions of the orbital period of observed sdBs with MS companions. The progenitor's initial mass changes from $1.0M_{\odot}$ (bottom) to $1.6M_{\odot}$ (top) for each line.

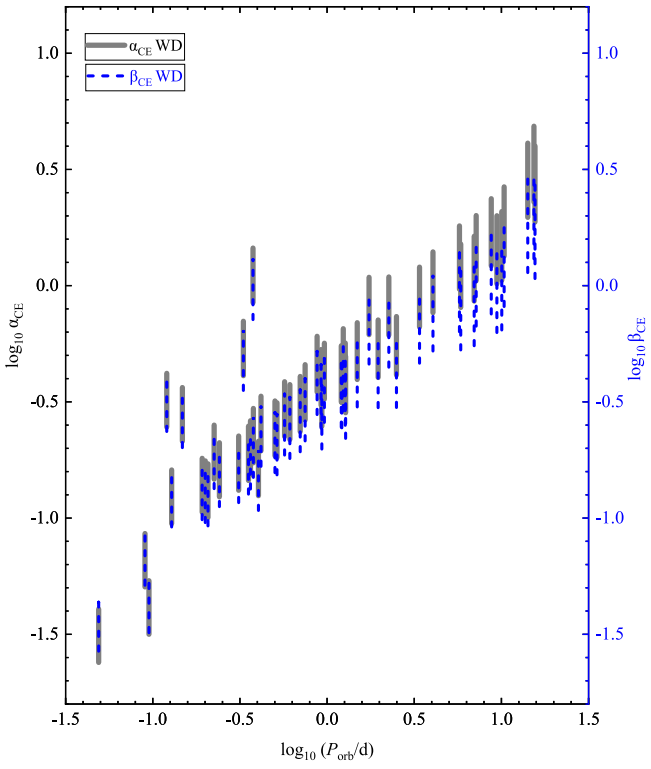

Figure 11. The CE efficiency parameters $\alpha_{\rm CE}$ (gray solid line) and $\beta_{\rm CE}$ (blue dashed line) as functions of the orbital period of observed sdBs with WD companions.

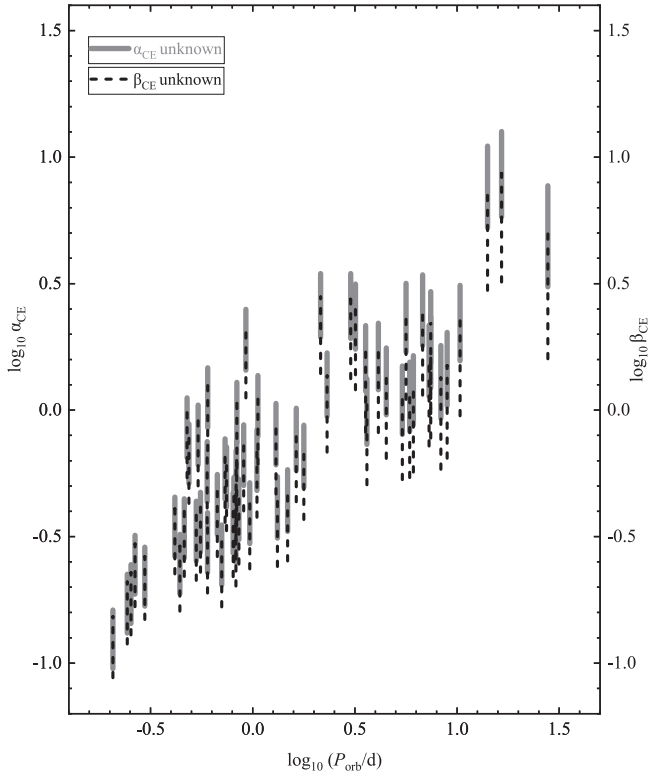

Figure 12. The CE efficiency parameters $\alpha_{\rm CE}$ (gray solid line) and $\beta_{\rm CE}$ (black dashed line) as functions of the orbital period of observed sdBs with unknown-type companions.

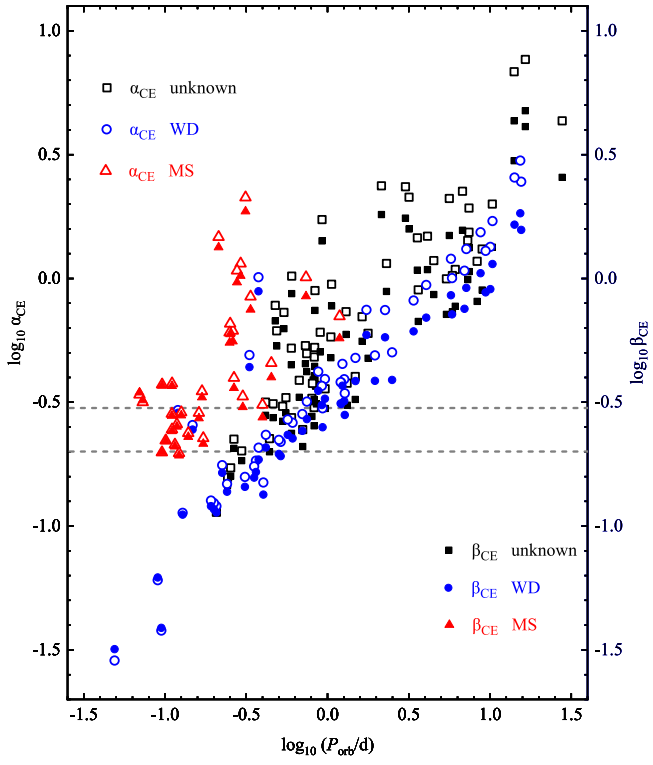

Figure 13. Weighted CE efficiency parameters $\alpha_{\rm CE}$ (open symbols) and $\beta_{\rm CE}$ (filled symbols) as functions of the orbital period of observed sdBs. Squares, circles, and triangles show the unknown-type, WD, and MS companions. Two horizontal thin-dashed lines are CE efficiency parameters of 0.2 and 0.3.

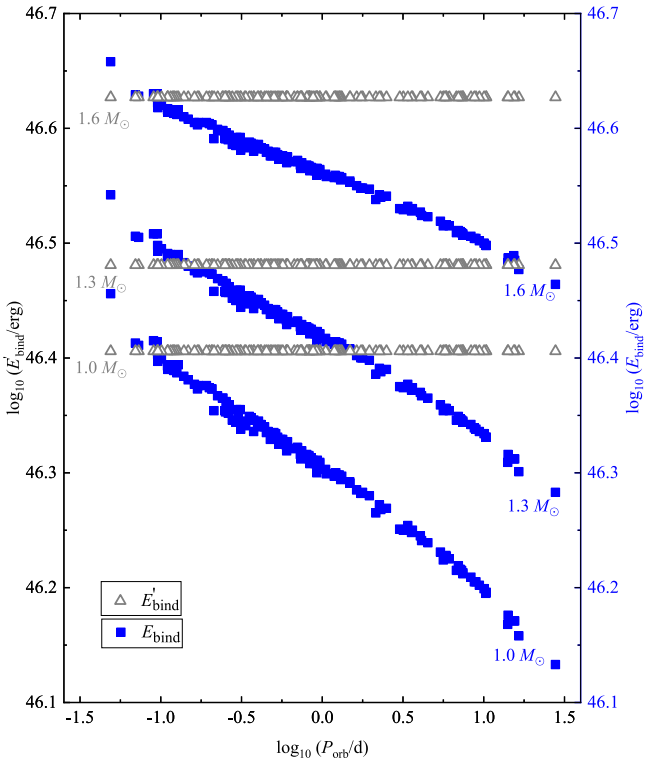

Figure 14. Binding energy as a function of the orbital period of sdBs. Gray open triangles show $E'_{\rm bind}$ as the integral of gravitational and internal energies from the progenitor's core to surface. Blue filled squares indicate the binding energy $E_{\rm bind}$ containing total energy, gravitational plus internal, from our adiabatic mass-loss model. $E_{\rm bind}$ represents both the rebalance of the remnant after mass ejection and the companion's effect.

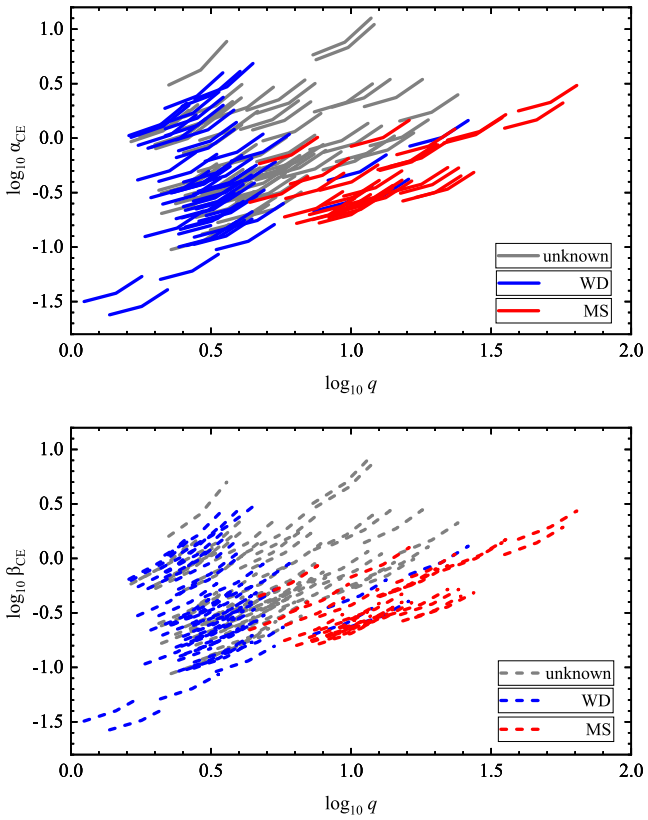

Figure 15. CE efficiency parameters as a function of mass ratio $q = M_{1i}/M_2$. The upper panel corresponds to the binding energy from standard prescription while that of the lower panel from total energy changes. A similar $\log 1/q$ versus $\log \alpha_{\rm CE}$ anticorrelation for postasymptotic giant branch binaries was explored by De Marco et al. (2011).

progenitors (Figures 10–11). If the above assumption is true we can connect the top part of the leftmost dashed line and the bottom part of the rightmost dashed line in these figures. Consequently, we can find a constant $\log_{10}\beta_{\rm CE} \approxeq -0.3$ for sdBs with an MS companion and from $\log_{10}\beta_{\rm CE} \approxeq -0.8$ to $\log_{10}\beta_{\rm CE} \approxeq -0.2$ for sdBs with a WD companion (abandoning the three leftmost objects might come from nondegenerate progenitors and the three rightmost objects with orbital periods longer than 10 days in Figure 11). In other words, the full orbital period range of sdBs can be covered within that CE efficiency parameter range. A concluding answer needs detailed binary population synthesis studies addressing the full range of the progenitors, metallicity, effects in this study, and more strict observation as discussed.

5. Summary and Conclusions

In this paper we calculate a binding energy $E_{\rm bind}$ that differs from previous studies by tracing the change of the total energy based on our adiabatic mass-loss model. For comparison, we also calculate the normal binding energy $E'_{\rm bind}$ through integrating the total energy from the core to the surface. We assume the outcome of CEE is determined by energy conservation and when both components shrink within their Roche lobes. We have found that the remnant core radius can vary by orders of magnitude although the remnant core mass is almost the same. The remnant core mass is slightly larger than the helium core. We examine short orbital period sdBs to estimate CE efficiency parameters with different binding energy calculation methods. The CE efficiency parameter is normally defined as $\alpha_{\rm CE}$ in the standard energy Equation (5).

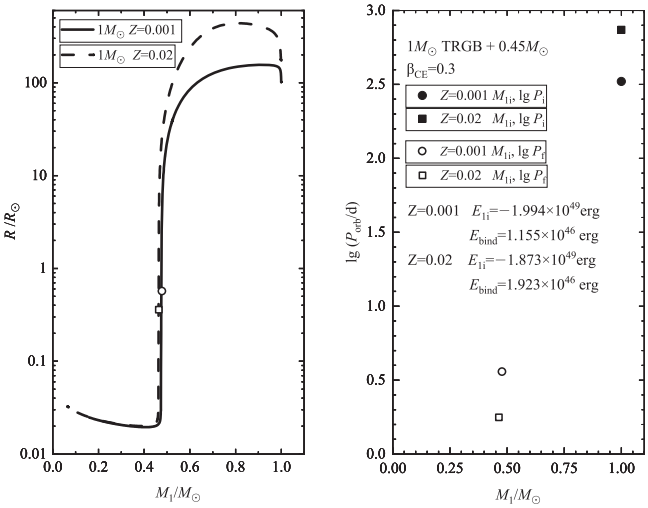

Figure 16. Metallicity dependence of the radius response (left panel) and the initial final mass and orbital period (right panel). The solid line and dashed line show the radius response of stars with $Z = 0.001$ and $Z = 0.02$. The solid and open symbols (squares for Z=0.02 and dots for $Z = 0.001$) are the initial and final mass and orbital period. Metal-poor stars are more compact and can shrink to their Roche lobes earlier than metal-rich stars.

We write the CE efficiency parameter as $\beta_{\rm CE}$ for our binding energy method. For shorter orbital period sdBs, the binding energy is almost the same and we find the difference between $\alpha_{\rm CE}$ and $\beta_{\rm CE}$ is small. For longer orbital period sdBs in our samples, we have found that the binding energy can differ by up to a factor

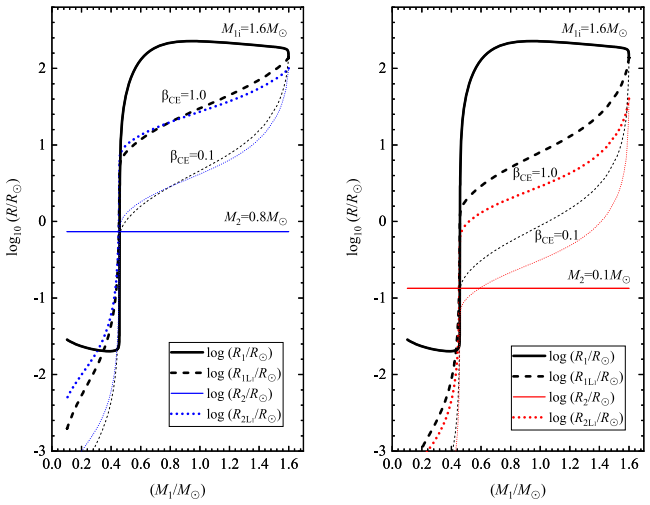

Figure 17. The remnant radius and Roche-lobe radius as a function of mass. Left and right panels are a 1.6 $M_\odot$ TRGB star with a 0.8 and a 0.1 $M_\odot$ MS companion. The black solid line is the radius response of the donor star. Dashed and dotted lines are the Roche-lobe radius of the donor and the companion. Thick and thin lines show the CE efficiency parameters of 1.0 and 0.1.

of 2. The CE efficiency parameter $\beta_{\rm CE}$ becomes smaller than $\alpha_{\rm CE}$ for final orbital periods $\log_{10} P_{\rm orb}/{\rm d} > -0.5$. A shallower slope for $\log_{10}\beta_{\rm CE}$ against $\log_{10} P_{\rm orb}$ than that for $\log_{10}\alpha_{\rm CE}$ is found for sdBs with all types of companion. We also find a $\log q$ and $\log\alpha_{\rm CE}$ linear correlation in sdBs similar to what De Marco et al. (2011) found in the post-AGB binaries.

To constrain the CEE physics more precisely, Hall & Tout (2014) improved the core radius fit through detailed stellar model calculations. Politano (2021) improved the radius at the mass–radius flat range (Terman & Taam 1996) by studying planetary nebulae with binary cores. De Marco et al. (2011) and Loveridge et al. (2011) provide useful constraints on the efficiency parameter $\alpha_{\rm CE}$ and structure parameter λ or the binding energy as a function of the stellar mass and evolutionary stage. However, our approach differs from earlier studies. We calculate the new binding energy $E_{\rm bind}$ by tracing the difference between the initial and final total energy of the donor star so that the influence of the companion mass on the binding energy is addressed. For more-massive close binaries, such as those with black holes or neutron stars, that come from more-massive progenitors than sdBs, the difference between $E_{\rm bind}$ and $E'_{\rm bind}$ is probably more important. Effects such as launching of jets may also play an important role (Soker 2022).

Different studies constraining the outcome of CEE process, such as our method, are important for binary population synthesis studies. More pre- and post-CE binary observations with more accurate orbital and structure parameters, as well as metallicity, are also of benefit. We shall present the grid of the CE efficiency parameters and other remnant information with different donor masses and evolutionary stages in the future.

The authors thank the anonymous referee for the helpful comments and suggested improvements. This project is supported by National Key R&D Program of China (2021YFA1600400/3) and National Natural Science Foundation of China (grants No. 12173081, 12090040/3, 11733008, 12125303, 11673058), Yunnan Fundamental Research Projects (grant No. 202101AV 070001), the key research program of frontier sciences, CAS, No. ZDBS-LY-7005, and CAS, "Light of West China Program". H.G. thanks the institute of astronomy, University of Cambridge for hosting the one year visiting. H.G. also thanks Prof. Ronald F Webbink for helpful suggestions. C.A.T. thanks Churchill College for his fellowship. D.J. acknowledge the science research grants No. 12073070 and CMS-CSST-2021-A08. Zhenwei Li acknowledges the science research grants No. 12103086, 202101AU070276.

ORCID iDs

Hongwei Ge https://orcid.org/0000-0002-6398-0195
Christopher A. Tout https://orcid.org/0000-0002-1556-9449
Xuefei Chen https://orcid.org/0000-0001-5284-8001
Matthias U. Kruckow https://orcid.org/0000-0001-9331-0400
Dengkai Jiang https://orcid.org/0000-0003-4265-7783
Zhenwei Li https://orcid.org/0000-0002-1421-4427
Zhengwei Liu https://orcid.org/0000-0002-7909-4171
Zhanwen Han https://orcid.org/0000-0001-9204-7778

References

Abbott, B. P., Abbott, R., Abbott, T. D., et al. 2016, PhRvL, 116, 131103
Abbott, B. P., Abbott, R., Abbott, T. D., et al. 2017, ApJL, 848, L12
Abbott, R., Abbott, T. D., Abraham, S., et al. 2021, PhRvX, 11, 021053
Blagorodnova, N., Klencki, J., Pejcha, O., et al. 2021, A&A, 653, A134
Chen, W.-C. 2020, ApJ, 896, 129
Chen, X., & Han, Z. 2003, MNRAS, 341, 662
Chen, X., & Han, Z. 2008, MNRAS, 387, 1416
de Kool, M. 1990, ApJ, 358, 189
De Marco, O., Passy, J.-C., Moe, M., et al. 2011, MNRAS, 411, 2277
Deloye, C. J., & Taam, R. E. 2010, ApJL, 719, L28
Dewi, J. D. M., & Tauris, T. M. 2000, A&A, 360, 1043
Duchêne, G., & Kraus, A. 2013, ARA&A, 51, 269
Eggleton, P. P. 1971, MNRAS, 151, 351
Eggleton, P. P. 1972, MNRAS, 156, 361
Eggleton, P. P. 1973, MNRAS, 163, 279
Eggleton, P. P. 1983, ApJ, 268, 368
El-Badry, K., & Quataert, E. 2021, MNRAS, 502, 3436
Ferguson, H. C., Davidsen, A. F., Kriss, G. A., et al. 1991, ApJL, 382, L69
Fontaine, G., Brassard, P., Charpinet, S., et al. 2003, ApJ, 597, 518
Fontaine, G., Brassard, P., Charpinet, S., et al. 2012, A&A, 539, A12
Ge, H., Hjellming, M. S., Webbink, R. F., Chen, X., & Han, Z. 2010a, ApJ, 717, 724
Ge, H., Webbink, R. F., Han, Z., & Chen, X. 2010b, Ap&SS, 329, 243
Ge, H., Webbink, R. F., Chen, X., & Han, Z. 2015, ApJ, 812, 40
Ge, H., Webbink, R. F., Chen, X., & Han, Z. 2020a, ApJ, 899, 132
Ge, H., Webbink, R. F., & Han, Z. 2020b, ApJS, 249, 9
Geier, S., Raddi, R., Gentile Fusillo, N. P., & Marsh, T. R. 2019, A&A, 621, A38
Gonzalez-Bolivar, M., De Marco, O., Lau, M. Y. M., Hirai, R., & Price, D. J. 2022, arXiv:2205.09749
Hall, P. D., & Tout, C. A. 2014, MNRAS, 444, 3209
Han, Z., Podsiadlowski, P., & Lynas-Gray, A. E. 2007, MNRAS, 380, 1098
Han, Z., Podsiadlowski, P., Maxted, P. F. L., & Marsh, T. R. 2003, MNRAS, 341, 669
Han, Z., Podsiadlowski, P., Maxted, P. F. L., Marsh, T. R., & Ivanova, N. 2002, MNRAS, 336, 449
Heber, U. 2009, ARA&A, 47, 211
Hernandez, M. S., Schreiber, M. R., Parsons, S. G., et al. 2021, MNRAS, 501, 1677
Hjellming, M. S., & Webbink, R. F. 1987, ApJ, 318, 794
Iben, I., Jr., & Tutukov, A. V. 1984, ApJS, 54, 335
Ivanova, N., Justham, S., & Ricker, P. 2020, Common Envelope Evolution (Bristol: IOP Publishing)
Justham, S., Wolf, C., Podsiadlowski, P., & Han, Z. 2009, A&A, 493, 1081
Kramer, M., Schneider, F. R. N., Ohlmann, S. T., et al. 2020, A&A, 642, A97
Kruckow, M. U. 2020, A&A, 639, A123
Kruckow, M. U., Tauris, T. M., Langer, N., et al. 2016, A&A, 596, A58
Kupfer, T., Geier, S., Heber, U., et al. 2015, A&A, 576, A44

Lagos, F., Schreiber, M. R., Parsons, S. G., Gänsicke, B. T., & Godoy, N. 2020, MNRAS, 499, L121
Lau, M. Y. M., Hirai, R., González-Bolívar, M., et al. 2022, MNRAS, 512, 5462
Leiner, E. M., & Geller, A. 2021, ApJ, 908, 229
Livio, M., & Soker, N. 1988, ApJ, 329, 764
Loveridge, A. J., van der Sluys, M. V., & Kalogera, V. 2011, ApJ, 743, 49
Luo, Y., Németh, P., Wang, K., Wang, X., & Han, Z. 2021, ApJS, 256, 28
Mandel, I., & Broekgaarden, F. S. 2022, LRR, 25, 1
Mandel, I., Müller, B., Riley, J., et al. 2021, MNRAS, 500, 1380
Marchant, P., Pappas, K. M. W., Gallegos-Garcia, M., et al. 2021, A&A, 650, A107
Maxted, P. F. L., Heber, U., Marsh, T. R., & North, R. C. 2001, MNRAS, 326, 1391
Misra, D., Fragos, T., Tauris, T. M., Zapartas, E., & Aguilera-Dena, D. R. 2020, A&A, 642, A174
Moe, M., & Di Stefano, R. 2017, ApJS, 230, 15
Nelemans, G., Yungelson, L. R., & Portegies Zwart, S. F. 2001, A&A, 375, 890
Paczynski, B. 1976, in IAU Symp. 73, Structure and Evolution of Close Binary Systems, Vol. 73, ed. P. Eggleton, S. Mitton, & J. Whelan (Dordrecht: Reidel), 75
Pavlovskii, K., & Ivanova, N. 2015, MNRAS, 449, 4415
Pavlovskii, K., Ivanova, N., Belczynski, K., & Van, K. X. 2017, MNRAS, 465, 2092
Paxton, B. 2004, PASP, 116, 699
Politano, M. 2021, A&A, 648, L6
Pols, O. R., Schröder, K.-P., Hurley, J. R., Tout, C. A., & Eggleton, P. P. 1998, MNRAS, 298, 525
Portegies Zwart, S. F., & Yungelson, L. R. 1998, A&A, 332, 173
Ricker, P. M., & Taam, R. E. 2012, ApJ, 746, 74
Ricker, P. M., Timmes, F. X., Taam, R. E., & Webbink, R. F. 2019, IAUS, 346, 449
Sand, C., Ohlmann, S. T., Schneider, F. R. N., Pakmor, R., & Röpke, F. K. 2020, A&A, 644, A60
Sen, K., Langer, N., Marchant, P., et al. 2022, A&A, 659, A98
Shao, Y., & Li, X.-D. 2021, ApJ, 920, 81
Smedley, S. L., Tout, C. A., Ferrario, L., & Wickramasinghe, D. T. 2014, MNRAS, 437, 2217
Soberman, G. E., Phinney, E. S., & van den Heuvel, E. P. J. 1997, A&A, 327, 620
Soker, N. 1998, AJ, 116, 1308
Soker, N. 2022, RAA, 22, 055010
Taam, R. E., & Sandquist, E. L. 2000, ARA&A, 38, 113
Terman, J. L., & Taam, R. E. 1996, ApJ, 458, 692
Vigna-Gómez, A., MacLeod, M., Neijssel, C. J., et al. 2020, PASA, 37, e038
Vos, J., Bobrick, A., & Vučković, M. 2020, A&A, 641, A163
Wang, B. 2018, RAA, 18, 049
Wang, B., & Liu, D. 2020, RAA, 20, 135
Webbink, R. F. 1975, PhD thesis, Univ. Cambridge
Webbink, R. F. 1984, ApJ, 277, 355
Webbink, R. F. 2008, in Short-Period Binary Stars: Observations, Analyses, and Results, ed. E. F. Milone, D. A. Leahy, & D. W. Hobill (Berlin: Springer), 233
Wilson, E. C., & Nordhaus, J. 2022, arXiv:2203.06091
Wu, Y., Chen, X., Li, Z., & Han, Z. 2018, A&A, 618, A14
Xu, X.-J., & Li, X.-D. 2010, ApJ, 716, 114
Zapartas, E., de Mink, S. E., Justham, S., et al. 2021, A&A, 645, A6
Zhang, Y., Chen, H.-L., Xiong, H., Chen, X., & Han, Z. 2021, MNRAS, 505, 3514
Zorotovic, M., Schreiber, M. R., Gänsicke, B. T., & Nebot Gómez-Morán, A. 2010, A&A, 520, A86